MODELING OF WAVES & CURRENTS AROUND POROUS SUBMERGED BREAKWATERS

Roshan Suminda Ranasinghe[1], Shinji Sato[2] and Yoshimitsu Tajima[3]

Abstract

The evolution of waves and wave-induced currents over porous submerged breakwaters is studied by applying a numerical model based on a truncated version of Chen (2006) Boussinesq-type equations for waves and currents over porous bottoms. The equations of motion for the porous medium include an empirical Forchheimer-type term for laminar and turbulent frictional losses and an inertial term for acceleration effects following Sollitt and Cross (1972). Comparisons between simulations and new set of laboratory experimental data show excellent agreement for wave field in one-dimensional horizontal wave propagation and qualitatively good agreement for wave and current field in horizontal two-dimensional wave propagation.

Key words: Boussinesq-type model, porous media, porous damping, submerged breakwaters, turbulent kinetic energy equation, nearshore currents

1. Introduction

The Boussinesq-type model equations for studying waves and currents around coastal structures have made remarkable advance during the past few decades. However, contrast to the fast development in modeling of hydrodynamics around impermeable structures, that of porous bottom or porous structures have been very slow, inevitably due to the uncertainty on determination of a few empirical coefficients associated with porous media. Most of the coastal structures such as groins, seawalls and offshore breakwaters are constructed with rubble, rocks or concrete blocks to withstand the forces generated by breaking waves and provide sufficient dissipation by turbulence in the interstices. As submerged breakwaters result primarily in wave dissipation through wave breaking over the structure, bottom friction and turbulence in porous layer, it is essential to include porous damping in modeling waves and currents around these structures.

A few mathematical models have been proposed to predict wave-current interaction with permeable beds and structures recently. Kabayashi (1986) applied a permeable-bed model based on the nonlinear shallow water wave equation and accordingly ignored frequency dispersion entirely. Rajanakamthorn et al. (1990) in their work proposed a mathematical model for evolution of waves on permeable beds based on the mild-slope equation. However their model is limited to small amplitude waves propagating over gentle slopes of uniform porous beds. Water wave interactions with porous seabeds were investigated theoretically and experimentally by Gu and Wang (1991) extending the porous flow model developed by Sollitt and Cross (1972). They pointed out the importance of including nonlinear and inertial resistance forces in porous flow models and derived a complex wave dispersion equation for waves propagating over porous media.

Flaten and Rigg (1991) were the first to propose Boussinesq-type model for evolution of waves over porous bed in shallow water with an asymptotic approach. Cruz et al. (1997) derived a set of 2DH Boussinesq equations over a porous bed of arbitrary thickness and tested their applicability on wave transformation over porous submerged breakwater with an opening for non-breaking waves. They incorporated frequency dispersion into the flow in porous media following the same approach of Madsen et al. (1991). Hsiao at al. (2002) presented a fully non-linear Boussinesq-type model, following the same approach of Nwogu (1993), to improve the dispersion properties inside the porous media and compared their model results with experimental data for the case of regular waves passing over the triangular porous

---

[1] Doctoral Student, Dept. of Civil Engineering, 7-3-1, Hongo, Bunkyo-ku, The University of Tokyo. 113-8656, Japan. sumindar@coastal.t.u-tokyo.ac.jp.
[2] Professor, ditto, sato@coastal.t.u-tokyo.ac.jp.
[3] Associate Professor, ditto, yoshitaji@coastal.t.u-tokyo.ac.jp.

submerged breakwater in 1DH. Though they achieved reasonably good results, their model makes the assumption of weak vertical vorticity, a limited range of particle size, and weak spatial variation of damping rates inside the porous layer. Very recently, Chen (2006) improved Hsiao et al. (2002) model by eliminating weak vertical vorticity assumption and retaining higher order porous damping terms in momentum equation. His model relaxes the assumption on the scaling of the linear damping term in the momentum conservation equation for the porous layer, and therefore it is applicable to a wide range relative porous layer thicknesses. Recognizing the importance of retaining the vertical vorticity in Boussinesq-type equations for the simulation of breaking induced nearshore circulations, Chen et al. (2003) have eliminated the z dependency in the fully nonlinear Boussinesq-type equations for impermeable beds by setting $z = z_\alpha$ in momentum conservation equation. Instead of choosing an arbitrary z, Chen (2006) opted to integrate momentum conservation equations for both water layer and porous layer. This resulted elimination of z dependency, at the same time retention of both the leading order and second order vertical vorticity terms. The fundamental properties for wave propagation (wave celerity, porous damping rates) of Chen (2006) model equations are investigated in Cruz and Chen (2006) for constant depth and horizontal porous interface. One of the desirable features of Chen (2006) model is its potential applicability to heterogeneous porous beds. Cruz and Chen (2007) discussed the heterogeneity in the hydraulic properties of porous layers, which could lead to spatial variation in the porous resistance.

Though most of the models have been tested for non-breaking wave transformation over porous submerged breakwaters; a few studies investigate the evolution of waves and wave-induced nearshore currents around these structures. Some exception are Johnson et al. (2005), and Johnson (2006) who validated a higher-order Boussinesq-type model (Karambas and Koutitas, 2002) with improved linear dispersion properties together with nonlinear long wave equation for porous media (Cruz. et al., 1997) using experimental data collected during the DELOS project. An eddy viscosity formulation is adopted in order to simulate the wave breaking induced energy dissipation (Kennedy et al., 2000).

The goal of the present study is to discuss the evolution of waves and wave-induced currents around submerged porous breakwaters and to validate a numerical model based on a truncated version of Chen (2006) equations coupled with a transport equation to compute turbulent kinetic energy hence energy dissipation due to wave breaking.

2. Description of the governing equations for waves and currents over porous beds

Figure 1 shows the definition of the variables and the Cartesian coordinate system, where (x,y) denote the horizontal coordinates, z is the vertical coordinate, and $z = \eta(x,y,t)$ is the free-surface elevation. The impermeable bottom boundary is at $z = h_b(x,y)$ and permeable interface at $z = h(x,y)$.
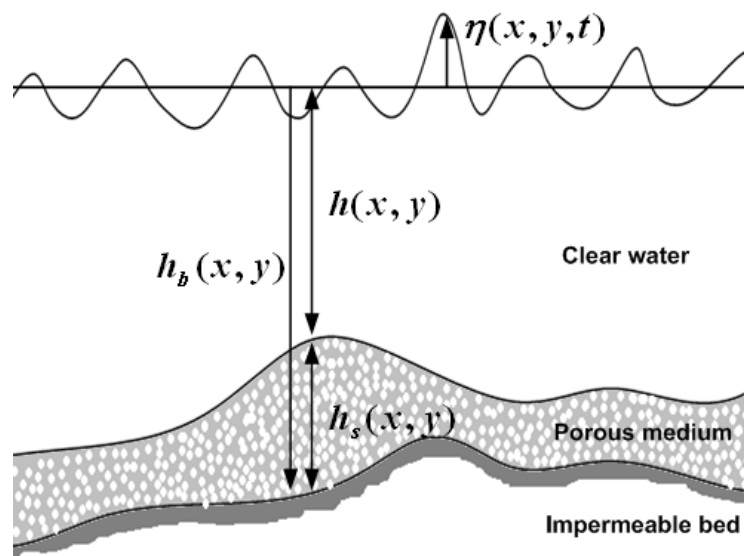

Figure 1. Definition sketch of variables associated with wave transformation over porous beds.

Dropping higher-order nonlinear terms and higher order porous damping terms, the mass conservation equation reads as:

$$\frac{\partial \eta}{\partial t} + \nabla.(\mathbf{M} + n\mathbf{M^s}) = 0 \tag{1}$$

where,

$$\mathbf{M} = (h + \varepsilon\eta)\left\{ \mathbf{u}_\alpha + \mu^2 \left[\left(\frac{z_\alpha^2}{2} - \frac{h^2}{6} \right) \nabla(\nabla.\mathbf{u}_\alpha) + \left(z_\alpha + \frac{h}{2} \right) \nabla\left(\nabla.(h\mathbf{u}_\alpha) + n\nabla.(h_s\mathbf{u}_\beta) \right) \right] \right\} \tag{2}$$

$$\mathbf{M^s} = h_s \left\{ \mathbf{u}_\beta + \mu^2 \left[\left(\frac{z_\beta^2}{2} - \frac{(h^2 + hh_b + h_b^2)}{6} \right) \nabla(\nabla.\mathbf{u}_\beta) + \left(z_\beta + \frac{(h+h_b)}{2} \right) \nabla\left(\nabla.(h_b\mathbf{u}_\beta) \right) \right] \right\} \tag{3}$$

The momentum conservation equation for the water layer can be written as:

$$\frac{\partial \mathbf{u}_\alpha}{\partial t} + \varepsilon(\mathbf{u}_\alpha.\nabla)\mathbf{u}_\alpha + \nabla\eta + \mu^2 \left\{ \frac{z_\alpha^2}{2} \nabla(\nabla.\mathbf{u}_{\alpha t}) + z_\alpha\nabla\left[\nabla.(h\mathbf{u}_{\alpha t}) + n\nabla.(h_s\mathbf{u}_{\beta t})\right] \right\} = 0 \tag{4}$$

And the momentum conservation equation for the porous layer can be written as:

$$\begin{aligned}
&\frac{\partial \mathbf{u}_\beta}{\partial t} + \delta(\mathbf{u}_\beta.\nabla)\mathbf{u}_\beta + \nabla\eta + \frac{1}{\delta}R_\beta\mathbf{u}_\beta + \\
&\mu^2 \left\{ \begin{array}{l} \frac{z_\beta^2}{2}\nabla(\nabla.\mathbf{u}_{\beta t}) + z_\beta\nabla\left[\nabla.(h\mathbf{u}_{\alpha t})\right] + \nabla\left(\frac{h^2}{2}\nabla.\mathbf{u}_{\alpha t} \right) - \nabla\left[h\nabla.(h\mathbf{u}_{\alpha t})\right] - n\nabla\left[h\nabla.(h_s\mathbf{u}_{\beta t})\right] - \\ \nabla\left(\frac{h^2}{2}\nabla.\mathbf{u}_{\beta t} \right) + \nabla\left[h\nabla.(h_b\mathbf{u}_{\beta t})\right] \end{array} \right\} + \\
&\frac{\mu^2}{\delta} \left\{ \begin{array}{l} R_\beta \frac{z_\beta^2}{2}\nabla(\nabla.\mathbf{u}_\beta) + R_\beta z_\beta\nabla\left[\nabla.(h_b\mathbf{u}_\beta)\right] - \nabla\left(\frac{R_\beta h^2}{2}\nabla.\mathbf{u}_\beta \right) + \nabla\left[R_\beta h\nabla.(h_b\mathbf{u}_\beta)\right] + \\ \nabla R_\beta\left[\frac{1}{6}(h_b^2 + hh_b + h^2)\nabla.\mathbf{u}_\beta - \frac{1}{2}(h+h_b)\nabla.(h_b\mathbf{u}_\beta) \right] \end{array} \right\} = 0
\end{aligned} \tag{5}$$

where $\mathbf{u}_\alpha = (u_\alpha, v_\alpha)$ is the water particle velocity vector at $z = z_\alpha$ (inside water layer) and $\mathbf{u}_\beta = (u_\beta, v_\beta)$ is the water particle velocity vector at $z = z_\beta$ (inside permeable layer). The symbol n and $h_s(x,y)$ are the porosity and thickness of the permeable layer respectively, which could be arbitrary in x and y. R_β is the resistance force evaluated at $z = z_\beta$, as follows:

$$R_\beta = a_p + b_p |\mathbf{u^s}|\big|_{z=z_\beta} + C_A \frac{\partial}{\partial t} \tag{6}$$

$$|\mathbf{u^s}|\big|_{z=z_\beta} = \sqrt{u_\beta^2 + v_\beta^2 + \mu^2\left[z_\beta\nabla.u_\beta + \nabla.(h_s u_\beta)\right]^2} \tag{7}$$

where a_p and b_p are respectively the linear and nonlinear porous resistance coefficients, and C_A is the added mass coefficient. The porous resistance coefficients a_p and b_p are estimated from the following relationships:

$$a_p = \frac{n\nu}{K_p}, \quad b_p = \frac{C_f n^2}{\sqrt{K_p}} \tag{8}$$

The intrinsic permeability, K_p, added-mass coefficient, C_A, and nonlinear drag coefficient, C_f, are calculated by empirical formulae, suggested by van Gent (1995) as follows:

$$K_p = \frac{d_{50}^2 n^3}{\alpha_p (1-n)^2}, \quad C_A = C_m \frac{(1-n)}{n}, \quad C_f = \beta_p \frac{1-n}{n} \frac{\sqrt{K_p}}{d_{50}} \tag{9}$$

where d_{50} is the median diameter of permeable materials, α_p, β_p and C_m are empirical coefficients that, in principle, should be determined by experiments for given permeable material.

3. Properties of the numerical model

The terms ($\overline{\Lambda}_2, \overline{\Lambda}_3$ and $\overline{\Lambda}_4$ in Chen, 2006), which come from the contribution of the higher-order vertical vorticity in Rw^s to the pressure field in the porous layer, and the terms, which stem from $O(\mu^4)$ terms in the polynomial expansion of the horizontal velocity vector, $\mathbf{u^s}$ are ignored in the present model. Only the higher-order terms ($\overline{\Lambda}_1$ in Chen, 2006), which are yielded by the removal of z dependency (by depth integration) are retained in the momentum conservation equation for the porous medium.

Following the same idea of Nwogu (1993), appropriate values for z_α and z_β are determined so that optimal dispersion properties of the model are achieved over a wide range of depths. The properties of the model are compared with those of the exact dispersion relation for linear water waves propagating in a constant depth, h, overlying a permeable bed with a constant thickness, h_s, is given by Gu and Wang (1991) as follows:

$$\sigma^2 - gk\tanh kh = -\frac{in}{a_p/\sigma - i(1+C_A)}\tanh kh_s (gk - \sigma^2 \tanh kh) \tag{10}$$

in which k is a complex number ($k = k_r + ik_i$), where the real part of k, denotes the wave number and the imaginary part represents the spatial porous damping rate.

$$\eta(x,t) = ae^{i(k_r x + k_i x - \sigma t)} = e^{-k_i x}\left[ae^{i(k_r x - \sigma t)}\right] \tag{11}$$

Detailed analysis of the model equations for their fundamental properties of wave motion over porous media can be found in Cruz and Chen (2006).

4. Numerical model

The Boussinesq-type equations are solved in the time domain using a third-order Adams-Bashforth predictor step and a forth-order Adams-Moulton corrector step. The computational domain is discretized as a rectangular grid with grid sizes Δx and Δy, in the x and y directions, respectively. The equation variables $\eta, u_\alpha, v_\alpha, u_\beta$ and v_β are defined at the grid points in a staggered mesh as shown in Fig. 2. The water depth and surface elevations are defined at grid points (i, j), while the velocities are defined half a grid point on either side of the elevation grid points. The external boundaries of the computational domain correspond to velocity grid points. The first-order spatial derivatives are differenced to $O(\Delta x^4)$, which automatically eliminates the error terms that would be of the same form as the dispersive terms (Wei and Kirby, 1995). The second-order spatial derivatives are discretized to $O(\Delta x^2)$, while the advection terms are differenced with second-order upwind difference scheme.

4.1. Offshore open boundary

As there is significant wave reflection from the submerged breakwaters, it is essential to absorb the waves, which propagate back to the wave incident boundary to prevent buildup of wave energy inside the computational domain. This has been achieved with line boundary method proposed by Ishii et al. (1994).
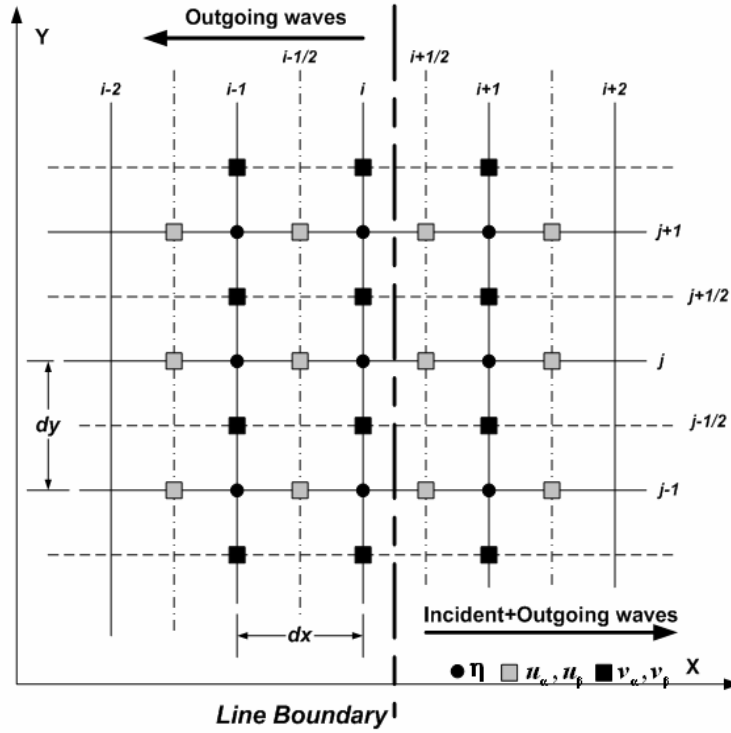

Figure 2. Definition sketch.

Here the neighboring grid points are divided into two types according to their position with respect to line boundary. Inside the line boundary, incident and outgoing waves are to be dealt with, whereas only outgoing waves exist outside the line boundary as shown in Fig.2. In the finite difference scheme, for the computation inside the line boundary, the parameters A_i (u_{ai}, v_{ai} or η_i), which are coming from outside the line boundary are added with $A_{i,in}$ and for the computation outside the line boundary, the parameters A_i, which are coming from inside the line boundary are subtracted with $A_{i,in}$.

4.2. Wave breaking induced energy dissipation

Following Kennedy et al. (2000), a simple eddy viscosity type of formulation is adopted to simulate energy dissipation due to wave breaking by introducing momentum-mixing terms into momentum conservation equations in x and y directions;

$$R_b^x = \frac{1}{(h+\eta)}\left(\left[\nu_t \left((h+\eta)u_\alpha\right)_x \right]_x + \frac{1}{2}\left[\nu_t \left((h+\eta)u_\alpha\right)_y + \nu_t \left((h+\eta)v_\alpha\right)_x \right]_y \right) \tag{12}$$

$$R_b^y = \frac{1}{(h+\eta)}\left(\left[\nu_t \left((h+\eta)v_\alpha\right)_y \right]_y + \frac{1}{2}\left[\nu_t \left((h+\eta)v_\alpha\right)_x + \nu_t \left((h+\eta)u_\alpha\right)_y \right]_x \right) \tag{13}$$

The magnitude of the eddy viscosity is computed using one equation turbulence closure model, in which the eddy viscosity is related to turbulent kinetic energy and turbulent length scale:

$$k_t + \mathbf{u}_s . \nabla k = \sigma \nabla . \nabla (v_t k) + B \frac{l_t^2}{\sqrt{C_D}} \left[\left(\frac{\partial u}{\partial z} \right)^2 + \left(\frac{\partial v}{\partial z} \right)^2 \right]_{z=\eta}^{3/2} - C_D \frac{k^{3/2}}{l_t} \qquad (14)$$

$$v_t = \sqrt{k} l_t \qquad (15)$$

The parameter B is introduced to ensure that turbulence is produced only when horizontal velocity at the wave crest, u_s, exceeds the phase velocity of the wave calculated from the linear wave theory. The length scale, l_t is set to be of the order of deep-water wave height, while an empirical coefficient, C_D, is set to be 0.02. We employed anisotropic eddy viscosity concept in 2DH model following Tajima et al. (2007). The model assumes that the eddy viscosity in the wave propagating direction should be characterized by the eddy viscosity generated by breaking waves while eddy viscosity features should not be that significant in the direction of wave crests. Based on such assumption they determined anisotropic eddy viscosity by:

$$\begin{pmatrix} v_{xx} & v_{xy} \\ v_{yx} & v_{yy} \end{pmatrix} = \begin{pmatrix} v_t \cos^2 \theta & v_{LK} \\ v_{LK} & v_t \sin^2 \theta \end{pmatrix} \qquad (16)$$

where, θ, is the angle between wave propagating direction and x axis. The square of wave angle ($\cos^2 \theta, \sin^2 \theta$) is introduced considering both the shear velocity and the turbulent length scale. v_{LK} is the well-known mixing term proposed by Larson and Kraus (1991).

$$v_{LK} = \Lambda H u_m \qquad (17)$$

where, Λ is a non-dimensional coefficient, H : local wave height, u_m : bottom wave orbital velocity.

5. Laboratory Experiments

Laboratory experiments were performed in a 30m long, 0.6m wide, 0.8m deep wave-current flume and a 11m long, 6.5m wide, 0.3m deep wave basin at the University of Tokyo. Two different permeable materials were used for the submerged breakwaters and the structural dimensions and the wave parameters associated with all the experiments are shown in Table.1.

Table 1. Structural dimensions and wave parameters associated with experiments.

Case No.	Deep water wave height (m)	Wave period (s)	Offshore water depth (m)	Freeboard (m)	Mean diameter of permeable material (m)	Remarks
Ex01_A01	0.033	1.00	0.255	0.055	0.02	Non-breaking, 1DH
Ex02_B03	0.034	1.25	0.248	0.148	0.02	Non-breaking, 1DH
Ex03_A01	0.041	1.00	0.300	0.028	0.012	Breaking, 1DH
Ex03_A02	0.041	1.00	0.300	0.028	Impermeable	Breaking, 1DH
Ex04_A02	0.039	1.25	0.275	0.03	0.012	Breaking, 1DH
Ex05_A01	0.038	1.00	0.275	0.03	0.012	Breaking, 1DH
Ex06_A01	0.028	1.00	0.218	0.025	0.012	Breaking, 2DH

The layouts of six different experimental set-ups are shown in Fig. 3. The length of the constant depth of the flume is 11.45m and the slope of the fixed bed is 1:30, whereas those are 1.5m and 1/20 of the wave basin. All the experiments were conducted with normal incident regular waves and the submerged breakwaters were not allowed to subject to wetting and drying coexisting field in any of the cases.

The water surface fluctuations were measured using capacitance-type wave gauges with a frequency of 100Hz, from which the wave heights and mean water levels are determined at those locations. The nearshore currents were visualized using particle tracking velocimetry (PTV) technique in wave basin experiments.
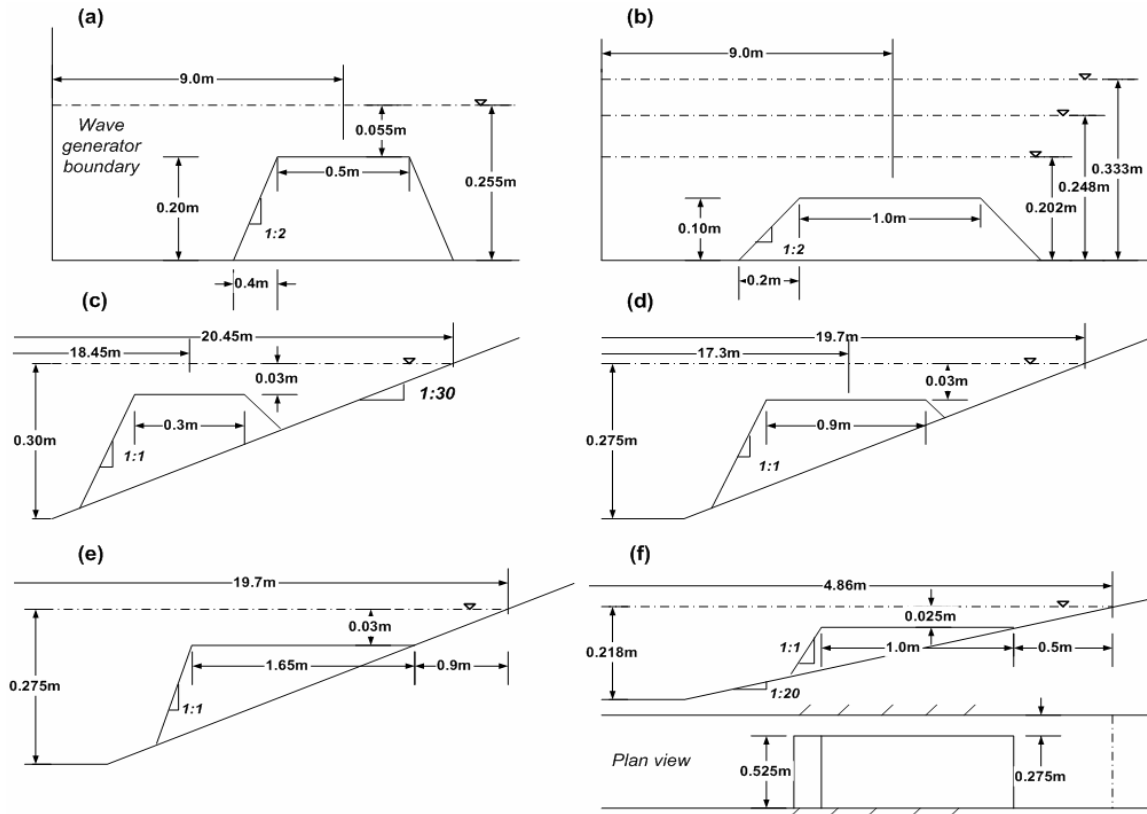
Figure 2. Layouts of the 6 different experimental setups.

6. Results and Discussion

The model results are firstly verified with data obtained from the wave-current flume experiments. Figure 4 shows the time series of observed (yellow circles) and simulated (blue line) free surface elevations at 9 different locations over a trapezoidal porous submerged mound placed under constant water depth of 0.255m and having a minimum freeboard of 0.055m (case Ex01_A01). The mean diameter and the porosity of the permeable material were found to be around 0.02m and 0.44 respectively. van Gent (1995) concluded that, though the coefficients α_p, β_p depend on parameters like shape, aspect ratio or the orientation of the permeable material, the values 1000 and 1.1 can be used for α_p, β_p respectively, if the characteristic length-scale the d_{50} is used. In addition, he suggested using a constant value for the empirical coefficient C_m of 0.34 for simplicity neglecting the complex dependency of coefficient C_A on the flow field. The following parameters are computed for the porous material used in cases Ex01_A01 and Ex02_B03 as suggested by van Gent (1995).

Intrinsic permeability, $K_p = 1.087 \times 10^{-7} \, \text{m}^2$
Added-mass coefficient, $C_A = 0.43$
Nonlinear drag coefficient, $C_f = 0.023$

Then the corresponding dimensional drag coefficients become:

$$a_p = 4.066 \, \text{s}^{-1}, \ b_p = 13.552 \, \text{m}^{-1} \tag{18}$$

The period of incident waves is 1.0s for the case Ex01_A01 and numerical computations are carried out with a space step of 0.0125m and a time step of 0.00667s. These are the space step and time step used for all the breaking and non-breaking 1.0s period waves. Numerical results show very good agreement with the

7

measured data except in the region behind the porous mound, where there exists a slight overestimation of the free water surface elevation. This could be probably due to the ignorance of higher-order porous damping rate terms, as the maximum porous layer thickness ratio, $r = h_s / h$ is as high as 3.63. It should also be noted that, in lee of the submerged mound nonlinear waves are decomposed into shorter waves as a result of energy transfer from primary wave component into its higher harmonics. Therefore wave dispersivity as well as nonlinearity could be influential in the simulations. Simulated in-phase water surface fluctuations (red lines) over impermeable submerged breakwater are also depicted here for comparison. It clearly explains the effectiveness of including porous damping terms in numerical simulation, when dealing with submerged breakwaters constructed with permeable materials.
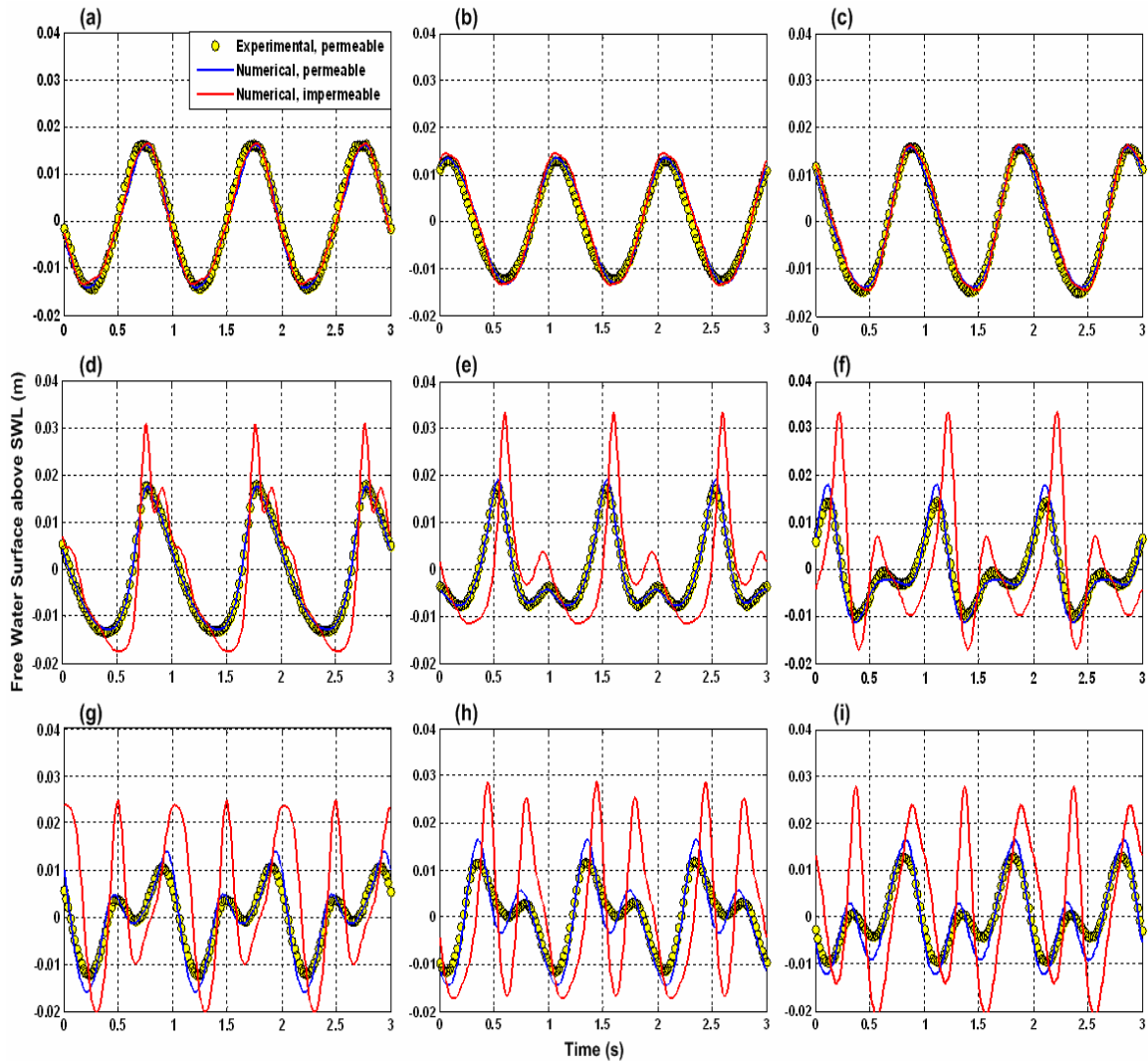

Figure 4. Simulated free water surface fluctuations at 8.0m(a), 8.4m(b), 8.6m(c), 8.8m(d), 9.2m(e), 9.4m(f), 9.6m(g), 10.0m(h), 10.4m(i) from wave generator boundary for case Ex01_A01

Time series of simulated and observed free water surface fluctuations for case Ex02_B03 are shown in Fig. 5. The wave period and the deep-water wave height in this case are 1.25s and 0.034m respectively. Numerical computations are carried out with a space step of 0.02m and a time step of 0.00833s for this case and the overall agreement of the simulated water level fluctuations with observed data seems to be confirmed. The wave is longer than the previous case, which makes the frequency dispersion characteristics become relatively less significant. Though the crest of the submerged mound of Ex02_B03 is wider than that of case Ex01_A01, the height of the mound is only 0.1m. On the other hand minimum freeboard is found to be 0.148m resulting weak nonlinear profiles for the waves as it could be clearly seen

from Fig. 5. The higher-order porous damping rate terms also play less significant role as the maximum porous layer thickness ratio, $r = h_s/h$ is 0.68.
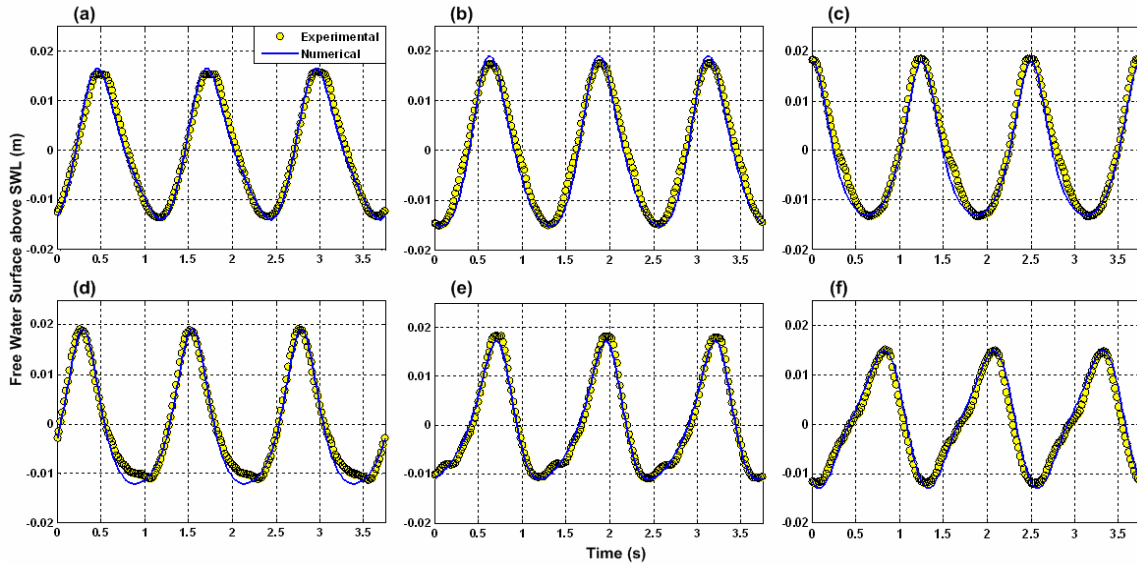

Figure 5. Simulated free water surface fluctuations at 8.0m(a), 8.4m(b), 8.8m(c), 9.2m(d), 9.6m(e), 10.0m(f) from wave generator boundary for case Ex02_B03

Then the evolution of breaking (surf-zone) waves over submerged breakwater in 1DH (wave flume experiments) is investigated. Four different experiment results were utilized for the verification (note that Ex03_A02 is conducted with an impermeable breakwater to compare the characteristics). The mean diameter and porosity of the permeable materials used in these experiments were found to be 0.012m and 0.44 respectively. Similar to previous cases, the following parameters are computed for the numerical model.

Intrinsic permeability, $K_p = 3.911 \times 10^{-08} \, \text{m}^2$
Added-mass coefficient, $C_A = 0.43$
Nonlinear drag coefficient, $C_f = 0.023$

The corresponding dimensional drag coefficients become:

$$a_p = 6.972 \, \text{s}^{-1}, \; b_p = 22.53 \, \text{m}^{-1} \tag{19}$$
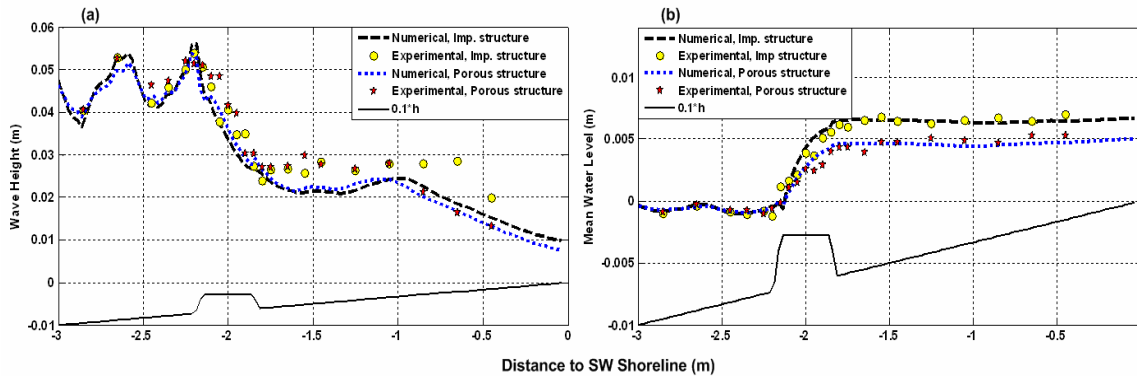

Figure 6. Simulated wave height distributions (a), and mean water level distributions (b) for cases Ex03_A01 and Ex03_A02

Figure 6 shows the observed and simulated wave height distribution (a) and the mean water level distribution (b) over a submerged breakwater (both permeable and impermeable) placed 2.0m offshore with a freeboard of 2.8cm. Prominent difference in the wave height distributions is not observed between permeable and impermeable condition, as the breaking criterion and the formulation for energy dissipation due to wave breaking is kept unchanged in the model. In addition to that narrow crest width (0.3m) makes the wave height reduction due to spatial porous damping become less significant compared that due to wave-breaking induced energy dissipation. Moreover, modeled wave heights are slightly underestimated in the lee of the breakwater particularly for case Ex03_A02 (impermeable), though the mean water levels show excellent agreement. Production of high turbulent kinetic energy leads to over-decaying of wave energy especially just behind the breakwater; hence insufficient recovery of the waves shoreward in the numerical model.
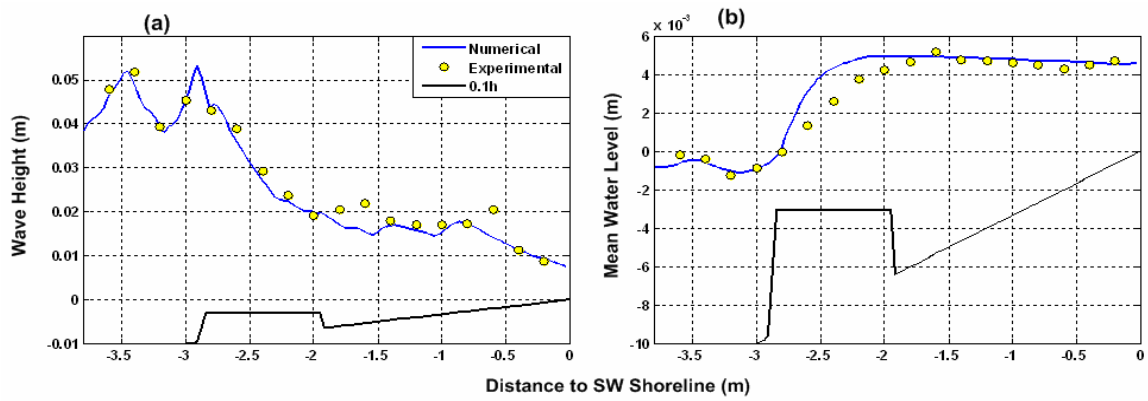

Figure 7. Simulated wave height distribution (a), and mean water level distribution (b) for case Ex04_A02
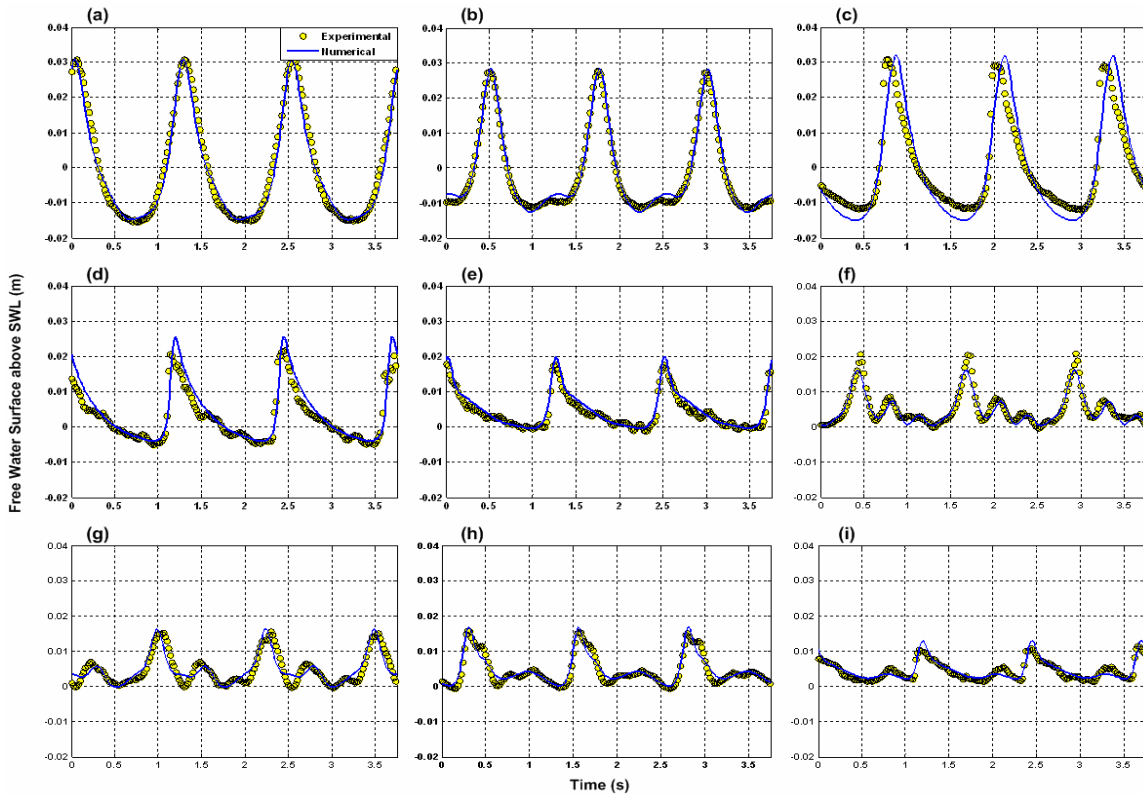

Figure 8. Simulated free water surface fluctuations at 3.6m(a), 3.2m(b), 2.8m(c), 2.4m(d), 2.0m(e), 1.6m(f), 1.2m(g), 0.8m(h), 0.4m(i) offshore from still water shoreline for case Ex04_A02

Interestingly mean water level reduction of about 25% is observed if the breakwater is considered to be porous. This is mainly due to the flow through the breakwater (partial free-path to undertow through porous medium), which declines piling-up of water behind the breakwater.

Figure 7 shows the wave height distribution (a) and mean water level distribution (b) over a broad-crested submerged breakwater under regular waves with a period of 1.25s). Fairly smooth decay of waves was observed with little recovery behind the breakwater. Model predicted the surface water fluctuations with excellent agreement with experimental data throughout the surf zone (Fig. 8). Even the generation of some higher harmonics was caught in the simulation though the waves could be considered as relatively long.
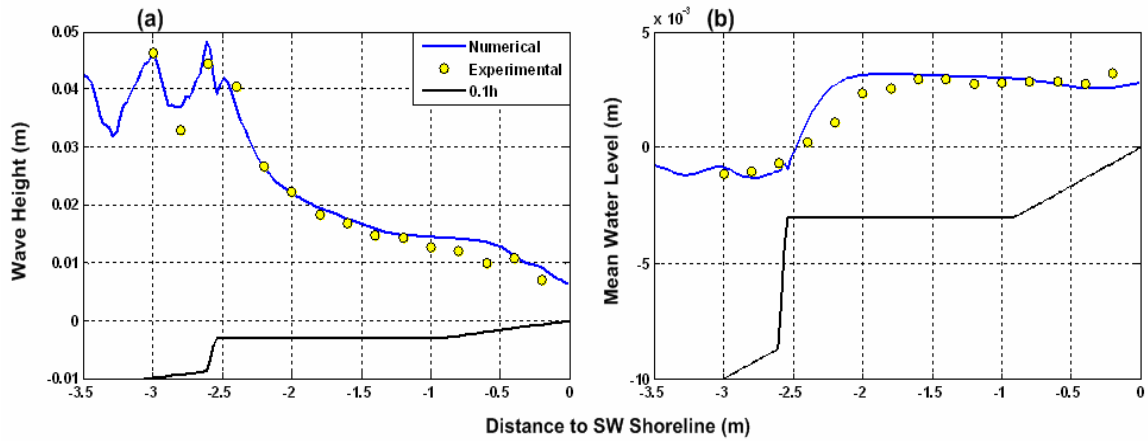

Figure 9. Simulated wave height distribution (a), and mean water level distribution (b) for case Ex05_A01
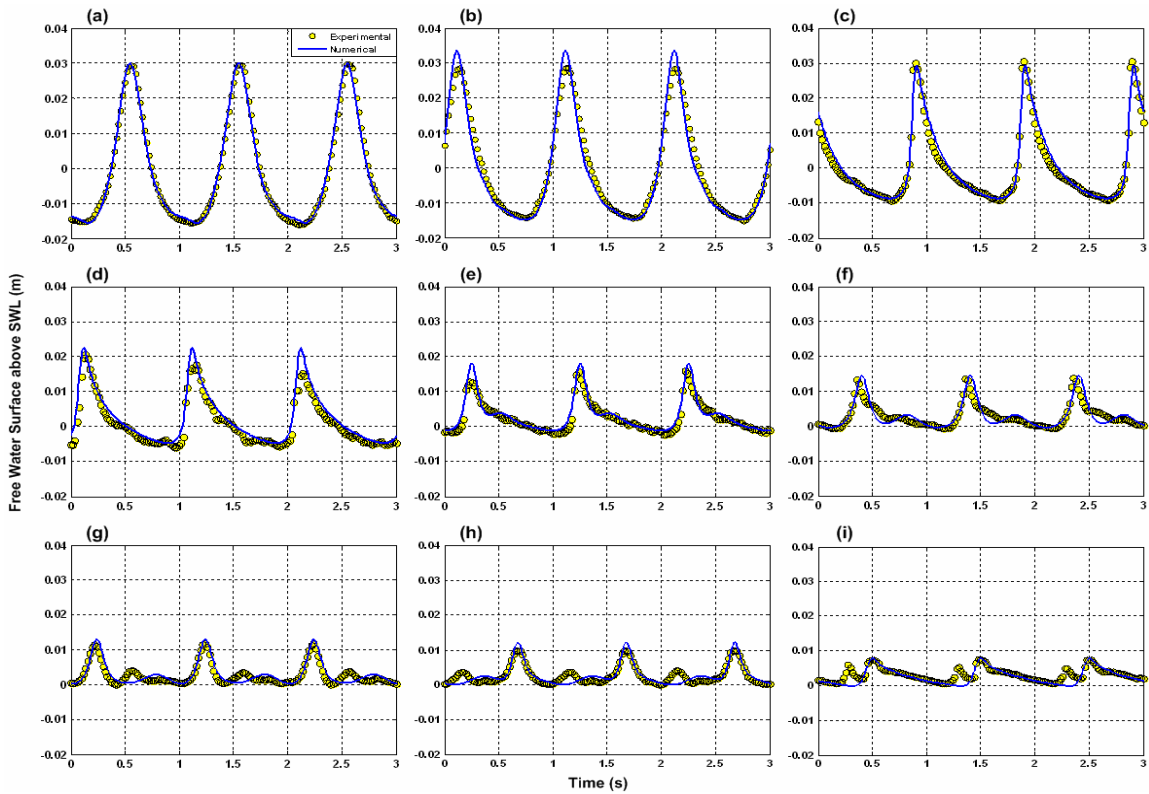

Figure 10. Simulated free water surface fluctuations at 3.0m(a), 2.6m(b), 2.4m(c), 2.2m(d), 1.8m(e), 1.4m(f), 1.0m(g), 0.6m(h), 0.2m(i) offshore from still water shoreline for case Ex05_A01

Numerical computations are also carried out for the wave evolution over a step-type submerged breakwater and the wave height distribution (a) and mean water level distribution (b) are shown in Fig. 9. Similar to case Ex04_A02, wave heights are well modeled, but the mean water levels are slightly overestimated over the stepped-crest of the breakwater. Time series of water level fluctuations also show some discrepancy near the shoreline, but the overall agreement is considered to be satisfactory.
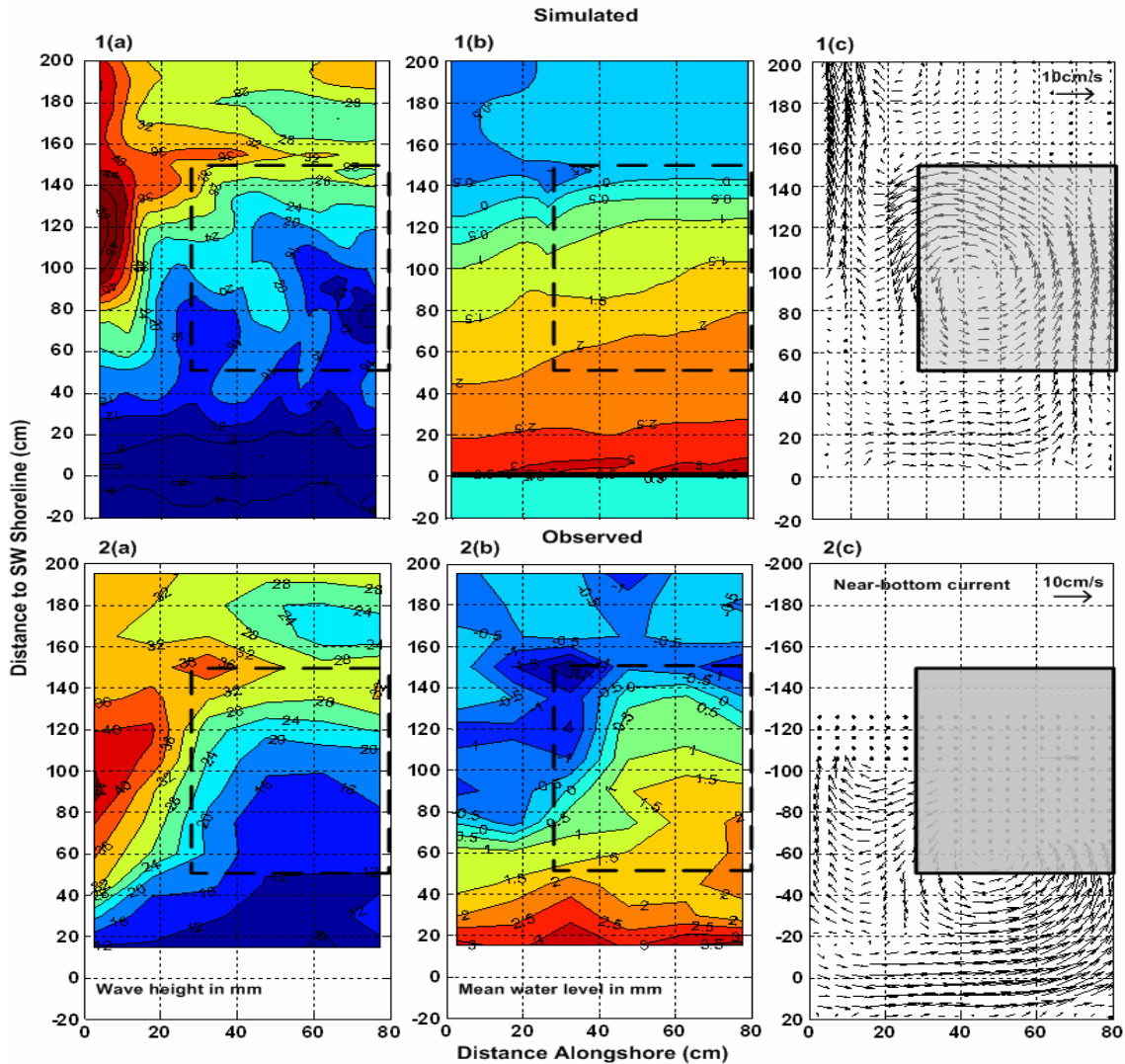

Figure 11. Simulated and observed wave height distribution (a), mean water level distribution (b), and nearshore current field (c) for case Ex06_A01

Simulated wave height distribution (a), mean water level distribution (b), and the nearshore current field (c) for case Ex06_A01 (infinite number of step-type submerged breakwaters 105cm long, having 55cm gaps between them) are depicted in Fig. 11 and compared with observed data [note that the 1(c) shows the depth-averaged current velocities, whereas 2(c) shows the nearbottom current velocities]. Significant alongshore variation of wave heights, and mean water levels is observed particularly in laboratory experiments, which drives the formulation of secondary circulation (converging) near the shoreline and interestingly, the direction of currents is found to be almost parallel to the alongshore direction. However, waves tend to break slightly earlier through the gap in the numerical simulation due to strong mixing of turbulent kinetic energy by advection and diffusion. This leads to relatively weaker alongshore variation in the wave height and mean water level distributions compared to observation, which weakens the strength of circulation currents behind the breakwater.

7. Conclusions

A 2DH model has been developed to simulate waves and currents around porous submerged breakwaters based on a truncated version of Chen (2006) Boussinesq-type equations for waves and currents over porous bottoms. Numerical simulations are carried out maintaining water layer throughout the space domain at every time step. *i.e.* porous breakwaters are not allowed to subject to wetting and drying coexisting field. Numerical computation results are verified with a new set of data collected using wave-current flume and wave basin experiments. Wave set up is reduced with a considerable degree if the breakwaters are of porous material, which is an essential characteristic for the formation of secondary circulation (converging) near the shoreline. Irrespective of the weakly nonlinear properties of the present model, 1DH model results show excellent agreement and 2DH model results show qualitatively good agreement with the observed data for variety of wave conditions and structural dimensions confirming selection of appropriate values for the empirical coefficients of the porous media and free parameters of the wave breaking-induced energy dissipation sub model.

References

Burcharth, H.F., Andersen, O.H. 1995. On the one-dimensional steady and unsteady porous flow equations. Coastal *Engineering*, 24, 233-257.

Chen, Q. 2006. Fully non-linear Boussinesq-type equations for waves and currents over porous beds. *Journal of Engineering Mechanics*, 132(2), 220-230.

Chen, Q., Kirby, J.T., Dalrymple, R.A., Shi, F., Thornton, E.B. 2003. Boussinesq modeling of longshore currents. *Journal of Geophysical Research*, 108(C11), 3362-3380.

Cruz, E.C., Chen, Q. 2006. Fundamental properties of Boussinesq-type equations for wave motion over a permeable bed. *Coastal Engineering Journal*, 48(3), 225-256.

Cruz, E.C., Chen, Q. 2007. Numerical modeling of nonlinear water waves over heterogeneous porous beds. *Ocean Engineering*, 34, 1303-1321.

Cruz, E.C., Isobe, M., Watanabe, A. 1997. Boussinesq equations for wave transformation on porous beds. *Coastal Engineering*, 30, 125-156.

Flatten, G, Rigg, O.B. 1991. Dispersive shallow water waves over a porous sea bed. *Coastal Engineering*, 15, 347-369.

Gu, Z., Wang, H. 1991. Gravity waves over porous bottoms. *Coastal Engineering,* 15, 497-524.

Hsiao, S.C., Liu, P.L.F., Chen, Y. 2002. Non-linear water waves over a permeable bed. *Proceedings, Royal Society of London*, Series A 458, 1291-1322.

Ishii, T., Isobe, M., Watanabe, A. 1994. Improved boundary conditions to a time-dependent mild-slope equation for random waves, in *Proc. 24th Int. Conf. Coastal Engineering,* ASCE, pp. 272-285.

Johnson, H.K. 2006. Wave modelling in the vicinity of submerged breakwaters. *Coastal Engineering*, 53, 39-48.

Johnson, H.K., Karambas, Th.V., Avgeris, I., Zanuttigh, B., Gonzalez-Marco, D., Caceres, I. 2005. Modelling of waves and currents around submerged breakwaters. *Coastal Engineering*, 52, 949-969.

Kabayashi, N. 1986. Closure to riprap stability under wave action. *Journal of Waterways, Port, Coastal and Ocean Engineering*, ASCE, 112, 673-681.

Karambas, Th.V., Koutitas, C. 2002. Surf and swash zone morphology evolution induced by nonlinear waves. *Journal of Waterways, Port, Coastal and Ocean Engineering*, ASCE, 128 (3), 102-113.

Kennedy, A.B., Chen, Q., Kirby, J.T., Dalrymple, R.A. 2000. Boussinesq modeling of wave transformation, breaking and run-up, I:1D," *Journal of waterways, Port, Coastal and Ocean Engineering*, ASCE, 126 (1), 39-47.

Nwogu, O.J. 1993. Alternative form of Boussinesq equations for nearshore wave propagation. *Journal of Waterways, Port, Coastal and Ocean Engineering*, ASCE, 119 (6), 618-638.

Rajanakamthorn, S., Isobe, M., Watanabe, A. 1990. Modelling of wave transformation on submerged breakwater. in *Proc. 23rd Int. Conf. Coastal Engineering,* ASCE, pp. 1060-1073.

Sollitt, C.K., Cross, R.H. 1972. Wave transmission through permeable breakwater. in *Proc. 13th Int. Conf. Coastal Engineering,* ASCE, pp. 1827-1846.

Tajima, Y., Sato, S., Shimozono, S., Isobe, M. 2007. Modelling of wave induced current around submerged detached breakwaters. *Proceedings, Coastal Structures '07,* ASCE, pp. 31-45.

van Gent, M.R.A. 1995a. Porous flow through rubble-mound material. *Journal of Waterways, Port, Coastal and Ocean Engineering*, ASCE, 121 (3), 176-181.

van Gent, M.R.A. 1995b. Wave interaction with permeable coastal structures. *PhD Thesis*, Delft University, Delft, The Netherlands.